Journal of Sound and Vibration 329 (2010) 4409–4421

Contents lists available at ScienceDirect

Journal of Sound and Vibration

journal homepage: www.elsevier.com/locate/jsvi

Dynamic analysis for a pair of spur gears with translational motion due to bearing deformation

Woohyung Kim [a], Hong Hee Yoo [b], Jintai Chung [a,*]

[a] Department of Mechanical Engineering, Hanyang University, 1271 Sa-3-dong, Sangnok-gu, Ansan, Kyeonggi-do 425-791, Republic of Korea
[b] School of Mechanical Engineering, Hanyang University, 17 Haengdang-dong, Seongdong-gu, Seoul 133-791, Republic of Korea

ARTICLE INFO

Article history:
Received 26 November 2009
Received in revised form
19 April 2010
Accepted 25 April 2010
Handling Editor: L.G. Tham
Available online 1 June 2010

ABSTRACT

In this study, the dynamic response of a pair of spur gears is analyzed when the gear set has translational motion due to bearing deformation. A new dynamic model for the gear set, considering translational motion, is proposed, in which the distance between the centers of a pinion and a gear varies with time. Therefore, the proposed model regards the pressure angle and the contact ratio as time-varying variables, while the previous model regards them as constants. After deriving nonlinear equations of motion for the gear set, the dynamic responses are computed by applying the Newmark time integration method. This paper claims that the new model produces more accurate dynamic responses in comparison to those of the previous model. Some dynamic response differences between the new and previous models are demonstrated, and the effects of damping and stiffness upon the dynamic responses are also investigated.

1. Introduction

Gears are considered to be one of the most important machine components and are widely used in various applications such as automobiles, aircrafts, heavy machinery, and marine vehicles. Gears have many functions, including reducing rotational speed, increasing available torque, or changing the direction of power transmission. In spite of the many functions of gears, noise, and vibration continue to cause major troubles within their applications. The noise and vibration from gears not only deteriorates the working environment, but also reduce the durability and reliability of machine systems. Noise and vibration are closely related to the dynamic behavior of a pair of gears caused by gear mesh deformation.

Many studies have been performed for the purpose of studying gear system dynamics. Related to gear dynamics, many efforts have been made to analyze the gear mesh stiffness and deformation caused by tooth contact. Cornell [1] and Tavakoli and Houser [2] modelled gear teeth as a cantilever beam. Huang and Liu [3] modelled a spur gear tooth as a variable cross-section Timoshenko beam for the dynamic analysis of spur gears of involute profiles. Because gear teeth have a non-uniform width with involute profiles, and because the contact position of the teeth varies with gear rotation, tooth stiffness, and deformation are complex periodic functions. Tooth deflection is influenced mainly by cantilever beam deflection, rigid-body tooth rotation, and contact deflection. Kuang and Lin [4] and Amabili and Fregolent [5] each presented a model of the mesh stiffness while considering the contact ratio. Their models have variable stiffness within a period, which can be divided into one-pair and two-pair contact stiffness. Kahraman [6] described the mesh stiffness as a

* Corresponding author. Tel.: +82 31 400 5287; fax: +82 31 406 5550.
E-mail address: jchung@hanyang.ac.kr (J. Chung).

0022-460X/$ - see front matter © 2010 Elsevier Ltd. All rights reserved.
doi:10.1016/j.jsv.2010.04.026

square wave function in order to analyze the nonlinear dynamic of the spur gear. Kahraman and Blankenship [7] investigated experimentally the influence of involute contact ratio on the torsional vibration behavior of a spur gear pair by measuring the dynamic transmission error of several gear pairs using a specially designed gear test rig. Velex and Maatar [8] introduced a mathematical gear model to analyze the influence of shape deviations and mounting errors on gear dynamics. Velex and Ajmi [9] established a relation between dynamic tooth loads and quasi-static transmission errors in helical gear sets.

On the other hand, mesh deformation is generally described with respect to the line of action. A simple model for mesh deformation was proposed by Ozguven and Houser [10] and showed that mesh deformation is generated by only the relative rotational gear motion. Kahraman and Singh [11] also used this same definition of mesh deformation, though they later modified the definition to consider the translational motion of the gears due to bearing deformations and transmission error [12]. However, they restricted the translational motion only in the direction along the line of action. By allowing the translational motion of the gears to occur within a two-dimensional plane, Kahraman [6] and Lin and Parker [13] proposed more realistic models for mesh deformation. Their models introduced pressure angle to the gear mesh deformation because these models include the planar motions of the gears, which is not along the line of action. Kahraman [14] also presented a three-dimensional model of a helical gear pair which accounts for the shaft and bearing flexibilities, and the dynamic coupling among the transverse, torsional, axial, and rocking motions due to the gear mesh. To the authors' knowledge, all previous studies have treated the pressure angle and the contact ratio as constants. In other words, the variations in both pressure angle and contact ratio were not considered when determining the gear mesh deformation. However, when a pair of gears possesses translational motion, the distance between the gear centers can be changed; therefore, it can be concluded that the pressure angle and the contact ratio are influenced by the center distance.

In order to consider translational motion due to bearing deformation, this study investigates the dynamic responses of a pair of spur gears consisting of a pinion and a gear. Considering the dependence of the pressure angle and the contact ratio on the translational motion of gears, a dynamic model for a pair of spur gears is newly proposed. Based on the proposed model, nonlinear and coupled equations of motion are derived. After expressing the equations within a matrix-vector form, the Newmark time integration method [15] is applied to obtain the dynamic responses for the pair of spur gears. Furthermore, the dynamic responses for the proposed model are compared to the responses for the previous model. In addition, the effects of various dampings, bearing stiffnesses, and gear mesh stiffnesses on the dynamic responses are studied.

2. Modelling of a pair of spur gears

Fig. 1 considers a pair of super gears consisting of a pinion and a gear. An external torque M exerts itself upon the pinion. The pinion has mass m_1 and a mass moment of inertia I_1 while the gear has mass m_2 and a mass moment of inertia I_2. The pinion and gear can possess rigid-body motion including translation and rotation. It is assumed in this paper that the gear set maintains only in-plane motion. This means that all motion occurs within the two-dimensional plane. The pinion and gear are supported by a pair of deformable bearings which can be modelled as linear springs and viscous dampers. The bearing stiffnesses of both the pinion and the gear are denoted by k_1 and k_2, respectively. The radial bearing damping coefficients of the pinion and gear are given by c_1 and c_2, respectively, and the torsional bearing damping coefficients are given by c_{t1} and c_{t2}. The pinion and gear, except for the teeth, are assumed to be rigid bodies. However, the teeth are regarded as flexible cantilever beams, because they are deformed by both bending and shear. The gear mesh stiffness is treated as a time-varying stiffness and will be discussed in more detail later.

The motion of the gear set can be defined with six generalized coordinates. The displacements of both the pinion and gear can be expressed via translational and rotational coordinates if they have planar motions. In Fig. 2, the dashed and solid lines represent the pair of spur gears before and after motion, respectively. Points O_1 and O_2 are the axis centers of the pinion and gear, which relocate to points C_1 and C_2 after the motion is completed. The mass centers of the pinion and gear are denoted by G_1 and G_2, respectively. The displacement of the pinion is given by translational coordinates, x_1 and y_1, and an angular coordinate θ_1, while the displacement of the gear is given by x_2, y_2, and θ_2. By denoting the displacement vectors

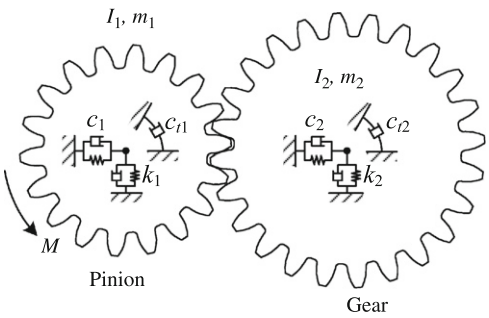

Fig. 1. Model of a pair of spur gears.

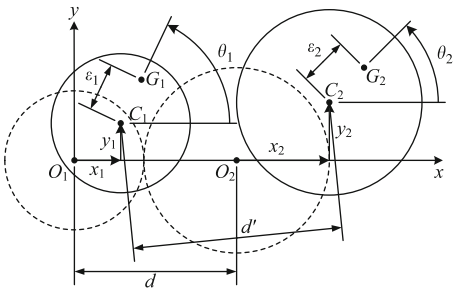

Fig. 2. Configuration and generalized coordinates for a pair of spur gears.

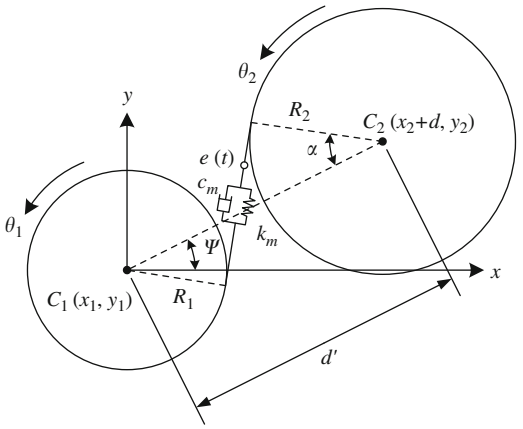

Fig. 3. Gear mesh model for a pair of spur gears.

for the mass centers of both the pinion and the gear by $\mathbf{r}_1$ and $\mathbf{r}_2$, these vectors are given by

$$\mathbf{r}_1 = (x_1+\varepsilon_1\cos\theta_1)\mathbf{i}+(y_1+\varepsilon_1\sin\theta_1)\mathbf{j} \quad \text{and} \quad \mathbf{r}_2 = (x_2+\varepsilon_2\cos\theta_2+d)\mathbf{i}+(y_2+\varepsilon_2\sin\theta_2)\mathbf{j} \tag{1}$$

where ε_1 and ε_2 are the eccentricities of the pinion and gear, and $\mathbf{i}$ and $\mathbf{j}$ are unit vectors along the x and y axes, respectively. Since the axis centers have displacements due to the translational motions of the pinion and gear, the center distance d changes to d' after the motion. The changed center distance d' is given by

$$d' = \sqrt{(x_2-x_1+d)^2+(y_2-y_1)^2} \tag{2}$$

A gear mesh model for the pair of spur gears in which the pinion and gear have translational rigid-body motions is presented in Fig. 3. The meshes of the pinion and gear may be modelled as time-varying gear mesh stiffness k_m, gear mesh damping coefficient c_m, and the transmission error on the line of action e. This line of action is defined as the common tangent line of the base circles in the gear set having involute tooth form. The pressure angle α is defined as the angle between the line of action and the direction of velocity at the pitch point. The angle ψ represents the position of the gear relative to the pinion, and the radii of the base circles for the pinion and the gear are denoted by R_1 and R_2, respectively.

The gear mesh deformation needs to be newly defined when the pinion and gear exhibit translational motions. For this case, the pressure angle is no longer constant. Recall that the pressure angle was regarded as a constant within all of the previous studies. The mesh deformation is defined along the line of action. Since the center distance d' is a function of x_1, y_1, x_2, and y_2, the pressure angle can be changed with time. In other words, when the pinion and gear exhibit translational motions, the pressure angle is not constant, but instead is a function of gear position. For the displacements in Fig. 3, the pressure angle may be expressed as

$$\alpha = \cos^{-1}\frac{R_1+R_2}{\sqrt{(x_2-x_1+d)^2+(y_2-y_1)^2}} \tag{3}$$

The position angle ψ is given by

$$\psi = \tan^{-1}\frac{y_2-y_1}{x_2-x_1+d} \tag{4}$$

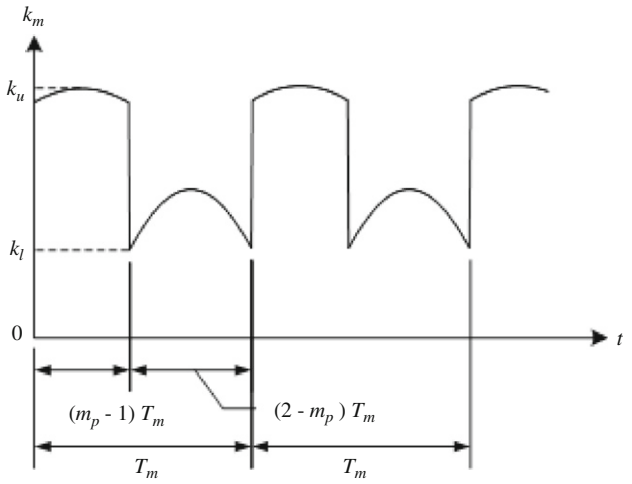

Fig. 4. Gear mesh stiffness with the contact ratio m_p and the mesh period T_m.

According to Kahraman [6] and Lin and Parker [13], the gear mesh deformation can be written as

$$\delta = (x_2 - x_1)\sin(\alpha - \psi) + (y_2 - y_1)\cos(\alpha - \psi) + R_1\theta_1 + R_2\theta_2 \tag{5}$$

where the transmission error e is neglected. The difference between the proposed and the previous mesh deformation equations is whether or not α and ψ are functions of the displacements of the pinion and the gear. In other words, this study considers the effects of the translational motions of the gear set on the pressure angle and the gear position angle, while the previous studies neglected these effects.

The modelling of gear mesh stiffness is important in analyzing the dynamic responses of the spur gear set. Even though many researchers have proposed various models for mesh stiffness, their models are not simple because they considered the deflections of gear teeth due to the bending and shear deformations, rigid-body rotation, and contact deformation of the tooth. Moreover, the contact ratio, which is the average mesh on the line of action, complicates mesh stiffness modelling. However, for simplicity of analysis, this study adopts the mesh stiffness model proposed by Kahraman [6]. In this model, mesh stiffness is described as a periodic function with a square wave form.

The contact ratio is closely related to the variation in gear mesh stiffness. In order for a pair of gears to obtain smooth continuous tooth action, when one pair of teeth loses contact with each other, a succeeding pair of teeth should come into engagement immediately. It is desirable that tooth contact overlaps as much as possible. A measure of this overlapping action is the contact ratio, which can be expressed by

$$m_p = \frac{\sqrt{A_1^2 - R_1^2} + \sqrt{A_2^2 - R_2^2} - d\sin\alpha}{p_b} \tag{6}$$

where A_1 and A_2 are the radii of the addendum circles for the pinion and the gear, and p_b is the base pitch.

This study adopts a time-varying gear mesh stiffness suggested by Tavakoli and Houser [2] and Chaari et al. [16]. A non-step model for gear mesh stiffness is presented in Fig. 4, when the spur gear set has the contact ratio m_p and a mesh period of T_m. The mesh stiffness with the mesh period T_m is divided into a one-pair and a two-pair contact zones. When the number of the gear teeth is N and the rotational speed of the gear is ω, the mesh period T_m is determined by the rotational speed of the gear and the number of teeth as follows:

$$T_m = 2\pi/N\omega \tag{7}$$

The time-varying gear mesh stiffness, shown in Fig. 4, is computed according to Tavakoli and Houser [2] and Chaari et al. [16]. The maximum value of stiffness, k_u, is in the two-pair contact zone while the minimum value, k_l, is in the one-pair contact zone. The proportions of the one-pair and two-pair contact zones are determined by the contact ratio. For any integer n, the two-pair contact zone is from $(n-1)T_m$ to $(m_p+n-2)T_m$ and the one-pair contact zone is from $(m_p+n-2)T_m$ to nT_m.

3. Derivation of the equations of motion

The equations of motion for a pair of spur gears, shown in Figs. 1–3, can be derived via the six generalized coordinates x_1, y_1, θ_1, x_2, y_2, and θ_2. After expressing the kinetic energy, the potential energy and Rayleigh's dissipation function of the spur gears in terms of the generalized coordinates, they are substituted into Lagrange's equation in order to obtain the

equations of motion. Since the gear set has planar motion, the kinetic energy T can be expressed as

$$T=(m_1\dot{\mathbf{r}}_1^2+I_1\dot{\theta}_1^2+m_2\dot{\mathbf{r}}_2^2+I_2\dot{\theta}_2^2)/2 \tag{8}$$

where the superimposed dot stands for differentiation with respect to time. When considering the bearings and tooth deformations, the potential energy V can be written as

$$V=[k_1(x_1^2+y_1^2)+k_2(x_2^2+y_2^2)+k_m\delta^2]/2 \tag{9}$$

Recall k_m is the time-varying stiffness and δ is a function of x_1, y_1, θ_1, x_2, y_2, and θ_2. Rayleigh's dissipation function due to the radial/torsional bearing damping and gear mesh damping is given by

$$F=[c_1(\dot{x}_1^2+\dot{y}_1^2)+c_2(\dot{x}_2^2+\dot{y}_2^2)+(c_{t1}\dot{\theta}_1^2+c_{t2}\dot{\theta}_2^2)+c_m\dot{\delta}^2]/2 \tag{10}$$

All of the generalized forces are zero except for the generalized force corresponding to the coordinate θ_1. Therefore, the generalized forces can be represented by

$$Q_{x_1}=Q_{y_1}=Q_{x_2}=Q_{y_2}=Q_{\theta_2}=0,\quad Q_{\theta_1}=M \tag{11}$$

The equations of motion are derived using Lagrange's equation, which is given by

$$\frac{\partial}{\partial t}\left(\frac{\partial T}{\partial \dot{q}_i}\right)+\frac{\partial F}{\partial \dot{q}_i}-\frac{\partial T}{\partial q_i}+\frac{\partial V}{\partial q_i}=Q_i \quad \text{for } q_i=x_1,\, y_1,\, \theta_1,\, x_2,\, y_2,\, \theta_2 \tag{12}$$

Substitution of Eqs. (8)–(11) into Eq. (12) leads to the following equations of motion:

$$\begin{aligned}&m_1(\ddot{x}_1-\varepsilon_1\ddot{\theta}_1\sin\theta_1-\varepsilon_1\dot{\theta}_1^2\cos\theta_1)+c_1\dot{x}_1\\&+c_m\delta_{,x_1}(\dot{x}_1\delta_{,x_1}+\dot{y}_1\delta_{,y_1}+\dot{\theta}_1\delta_{,\theta_1}+\dot{x}_2\delta_{,x_2}+\dot{y}_2\delta_{,y_2}+\dot{\theta}_2\delta_{,\theta_2})+k_1x_1+k_m\delta\delta_{,x_1}=0\end{aligned} \tag{13}$$

$$\begin{aligned}&m_1(\ddot{y}_1+\varepsilon_1\ddot{\theta}_1\cos\theta_1-\varepsilon_1\dot{\theta}_1^2\sin\theta_1)+c_1\dot{y}_1\\&+c_m\delta_{,y_1}(\dot{x}_1\delta_{,x_1}+\dot{y}_1\delta_{,y_1}+\dot{\theta}_1\delta_{,\theta_1}+\dot{x}_2\delta_{,x_2}+\dot{y}_2\delta_{,y_2}+\dot{\theta}_2\delta_{,\theta_2})+k_1y_1+k_m\delta\delta_{,y_1}=0\end{aligned} \tag{14}$$

$$\begin{aligned}&(I_1+m_1\varepsilon_1^2)\ddot{\theta}_1-m_1\varepsilon_1(\ddot{x}_1\sin\theta_1-\ddot{y}_1\cos\theta_1)+c_{t1}\dot{\theta}_1\\&+c_m\delta_{,\theta_1}(\dot{x}_1\delta_{,x_1}+\dot{y}_1\delta_{,y_1}+\dot{\theta}_1\delta_{,\theta_1}+\dot{x}_2\delta_{,x_2}+\dot{y}_2\delta_{,y_2}+\dot{\theta}_2\delta_{,\theta_2})+k_m\delta\delta_{,\theta_1}=M\end{aligned} \tag{15}$$

$$\begin{aligned}&m_2(\ddot{x}_2-\varepsilon_2\ddot{\theta}_2\sin\theta_2-\varepsilon_2\dot{\theta}_2^2\cos\theta_2)+c_2\dot{x}_2\\&+c_m\delta_{,x_2}(\dot{x}_1\delta_{,x_1}+\dot{y}_1\delta_{,y_1}+\dot{\theta}_1\delta_{,\theta_1}+\dot{x}_2\delta_{,x_2}+\dot{y}_2\delta_{,y_2}+\dot{\theta}_2\delta_{,\theta_2})+k_2x_2+k_m\delta\delta_{,x_2}=0\end{aligned} \tag{16}$$

$$\begin{aligned}&m_2(\ddot{y}_2+\varepsilon_2\ddot{\theta}_2\cos\theta_2-\varepsilon_2\dot{\theta}_2^2\sin\theta_2)+c_2\dot{y}_2\\&+c_m\delta_{,y_2}(\dot{x}_2\delta_{,x_1}+\dot{y}_1\delta_{,y_1}+\dot{\theta}_1\delta_{,\theta_1}+\dot{x}_2\delta_{,x_2}+\dot{y}_2\delta_{,y_2}+\dot{\theta}_2\delta_{,\theta_2})+k_2y_2+k_m\delta\delta_{,y_2}=0\end{aligned} \tag{17}$$

$$\begin{aligned}&(I_2+m_2\varepsilon_2^2)\ddot{\theta}_2-m_2\varepsilon_2(\ddot{x}_2\sin\theta_2-\ddot{y}_2\cos\theta_2)+c_{t2}\dot{\theta}_2\\&+c_m\delta_{,\theta_2}(\dot{x}_1\delta_{,x_1}+\dot{y}_1\delta_{,y_1}+\dot{\theta}_1\delta_{,\theta_1}+\dot{x}_2\delta_{,x_2}+\dot{y}_2\delta_{,y_2}+\dot{\theta}_2\delta_{,\theta_2})+k_m\delta\delta_{,\theta_2}=0\end{aligned} \tag{18}$$

where the comma denotes partial differentiation, e.g., $\delta_{,x_1}=\partial\delta/\partial x_1$

$$\delta_{,x_1}=-\sin(\alpha-\psi)+[(x_2-x_1)\cos(\alpha-\psi)-(y_2-y_1)\sin(\alpha-\psi)](\alpha_{,x_1}-\psi_{,x_1}) \tag{19}$$

$$\delta_{,y_1}=-\cos(\alpha-\psi)+[(x_2-x_1)\cos(\alpha-\psi)-(y_2-y_1)\sin(\alpha-\psi)](\alpha_{,y_1}-\psi_{,y_1}) \tag{20}$$

$$\delta_{,x_2}=\sin(\alpha-\psi)+[(x_2-x_1)\cos(\alpha-\psi)-(y_2-y_1)\sin(\alpha-\psi)](\alpha_{,x_2}-\psi_{,x_2}) \tag{21}$$

$$\delta_{,y_2}=\cos(\alpha-\psi)+[(x_2-x_1)\cos(\alpha-\psi)-(y_2-y_1)\sin(\alpha-\psi)](\alpha_{,y_2}-\psi_{,y_2}) \tag{22}$$

$$\delta_{,\theta_1}=R_1,\quad \delta_{,\theta_2}=R_2 \tag{23}$$

in which

$$\alpha_{,x_1}=-\alpha_{,x_2}=-\frac{(R_1+R_2)(x_2-x_1+d)}{[(x_2-x_1+d)^2+(y_2-y_1)^2]\sqrt{(x_2-x_1+d)^2+(y_2-y_1)^2-(R_1+R_2)^2}} \tag{24}$$

$$\alpha_{,y_1}=-\alpha_{,y_2}=-\frac{(R_1+R_2)(y_2-y_1)}{[(x_2-x_1+d)^2+(y_2-y_1)^2]\sqrt{(x_2-x_1+d)^2+(y_2-y_1)^2-(R_1+R_2)^2}} \tag{25}$$

$$\psi_{,x_1}=-\psi_{,x_2}=\frac{y_2-y_1}{(x_2-x_1+d)^2+(y_2-y_1)^2},\quad \psi_{,y_1}=-\psi_{,y_2}=-\frac{x_2-x_1+d}{(x_2-x_1+d)^2+(y_2-y_1)^2} \tag{26}$$

As shown in Eqs. (13)–(18), the equations of motion are nonlinear and are completely coupled to one another.

The derived nonlinear equations of motion can be represented in a matrix-vector form. This matrix-vector form is useful in computing dynamic responses when applying a numerical time integration algorithm. The matrix-vector form of the nonlinear equations can be written as

$$\mathbf{M}(\mathbf{x})\ddot{\mathbf{x}}+\mathbf{N}(\mathbf{x},\dot{\mathbf{x}})=\mathbf{f} \tag{27}$$

where $\mathbf{x}$ is the displacement vector, $\mathbf{M}$ is the mass matrix, $\mathbf{N}$ is the nonlinear internal force vector, and $\mathbf{f}$ is the external force vector as follows:

$$\mathbf{x}=\{x_1,y_1,\theta_1,x_2,y_2,\theta_2\}^{\mathrm{T}}$$

$$\mathbf{M}=\begin{bmatrix} m_1 & 0 & -m_1\varepsilon_1\sin\theta_1 & 0 & 0 & 0\\ 0 & m_1 & m_1\varepsilon_1\cos\theta_1 & 0 & 0 & 0\\ -m_1\varepsilon_1\sin\theta & m_1\varepsilon_1\cos\theta_1 & I_1+m_1\varepsilon_1^2 & 0 & 0 & 0\\ 0 & 0 & 0 & m_2 & 0 & -m_2\varepsilon_2\sin\theta_2\\ 0 & 0 & 0 & 0 & m_2 & m_2\varepsilon_2\cos\theta_2\\ 0 & 0 & 0 & -m_2\varepsilon_2\sin\theta_2 & m_2\varepsilon_2\cos\theta_2 & I_2+m_2\varepsilon_2^2 \end{bmatrix}$$

$$\mathbf{N}=\begin{Bmatrix} -m_1\varepsilon_1\dot{\theta}_1^2\cos\theta_{11}+c_1\dot{x}+c_m\delta_{,x_1}(\dot{x}_1\delta_{,x_1}+\dot{y}_1\delta_{,y_1}+\dot{\theta}_1\delta_{,\theta_1}+\dot{x}_2\delta_{,x_2}+\dot{y}_2\delta_{,y_2}+\dot{\theta}_2\delta_{,\theta_2})+k_1x_1+k_m\delta\delta_{,x_1}\\ -m_1\varepsilon_1\dot{\theta}_1^2\sin\theta_1+c_1\dot{y}_1+c_m\delta_{,y_1}(\dot{x}_1\delta_{,x_1}+\dot{y}_1\delta_{,y_1}+\dot{\theta}_1\delta_{,\theta_1}+\dot{x}_2\delta_{,x_2}+\dot{y}_2\delta_{,y_2}+\dot{\theta}_2\delta_{,\theta_2})+k_1y_1+k_m\delta\delta_{,y_1}\\ c_{t1}\dot{\theta}_1+c_m\delta_{,\theta_1}(\dot{x}_1\delta_{,x_1}+\dot{y}_1\delta_{,y_1}+\dot{\theta}_1\delta_{,\theta_1}+\dot{x}_2\delta_{,x_2}+\dot{y}_2\delta_{,y_2}+\dot{\theta}_2\delta_{,\theta_2})+k_m\delta\delta_{,\theta_1}\\ -m_2\varepsilon_2\dot{\theta}_2^2\cos\theta_2+c_2\dot{x}_2+c_m\delta_{,x_2}(\dot{x}_1\delta_{,x_1}+\dot{y}_1\delta_{,y_1}+\dot{\theta}_1\delta_{,\theta_1}+\dot{x}_2\delta_{,x_2}+\dot{y}_2\delta_{,y_2}+\dot{\theta}_2\delta_{,\theta_2})+k_2x_2+k_m\delta\delta_{,x_2}\\ -m_2\varepsilon_2\dot{\theta}_2^2\sin\theta_2+c_2\dot{y}_2+c_m\delta_{,y_2}(\dot{x}_2\delta_{,x_1}+\dot{y}_1\delta_{,y_1}+\dot{\theta}_1\delta_{,\theta_1}+\dot{x}_2\delta_{,x_2}+\dot{y}_2\delta_{,y_2}+\dot{\theta}_2\delta_{,\theta_2})+k_2y_2+k_m\delta\delta_{,y_2}\\ c_{t2}\dot{\theta}_2+c_m\delta_{,\theta_2}(\dot{x}_1\delta_{,x_1}+\dot{y}_1\delta_{,y_1}+\dot{\theta}_1\delta_{,\theta_1}+\dot{x}_2\delta_{,x_2}+\dot{y}_2\delta_{,y_2}+\dot{\theta}_2\delta_{,\theta_2})+k_m\delta\delta_{,\theta_2} \end{Bmatrix}$$

$$\mathbf{f}=\{0,0,M,0,0,0\}^{\mathrm{T}} \tag{28}$$

The displacement vector is a 1×6 column vector in which the elements are the generalized coordinates, x_1, y_1, θ_1, x_2, y_2, and θ_2. It should be noted that the mass matrix $\mathbf{M}$ is a function of the displacement vector $\mathbf{x}$, and the nonlinear internal force vector $\mathbf{N}$ is a function of the displacement vector $\mathbf{x}$ and the velocity vector $\dot{\mathbf{x}}$.

The equations of motion, as given in Eqs. (13)–(18), may be reduced to equations derived from previous studies. These studies assumed that the pressure angle was not influenced by the translational motion. In other words, the pressure angle and the contact ratio were independent of the translational coordinates, x_1, y_1, x_2, and y_2. Therefore, the pressure angle α was regarded as a constant and the position angle ψ was not introduced. When the pressure angle is assumed to be unaffected by the translational displacement, the pressure angle and the position angle can be given by

$$\alpha=\cos^{-1}(R_1+R_2)/d,\quad \psi=0 \tag{29}$$

and the gear mesh deformation of Eq. (5) is redefined as

$$\delta=(x_2-x_1)\sin\alpha+(y_2-y_1)\cos\alpha+R_1\theta_1+R_2\theta_2 \tag{30}$$

For this case, the governing equations of Eqs. (13)–(18) can be simplified into the following equations:

$$m_1(\ddot{x}_1-\varepsilon_1\ddot{\theta}_1\sin\theta_1-\varepsilon_1\dot{\theta}_1^2\cos\theta_1)+c_1\dot{x}_1-c_m\dot{\delta}\sin\alpha+k_1x_1-k_m\delta\sin\alpha=0 \tag{31}$$

$$m_1(\ddot{y}_1+\varepsilon_1\ddot{\theta}_1\cos\theta_1-\varepsilon_1\dot{\theta}_1^2\sin\theta_1)+c_1\dot{y}_1-c_m\dot{\delta}\cos\alpha+k_1y_1-k_m\delta\cos\alpha=0 \tag{32}$$

$$(I_1+m_1\varepsilon_1^2)\ddot{\theta}_1-m_1\varepsilon_1(\ddot{x}_1\sin\theta_1-\ddot{y}_1\cos\theta_1)+c_{t1}\dot{\theta}_1+c_mR_1\dot{\delta}+k_mR_1\delta=M \tag{33}$$

$$m_2(\ddot{x}_2-\varepsilon_2\ddot{\theta}_2\sin\theta_2-\varepsilon_2\dot{\theta}_2^2\cos\theta_2)+c_2\dot{x}_2+c_m\dot{\delta}\sin\alpha+k_2x_2+k_m\delta\sin\alpha=0 \tag{34}$$

$$m_2(\ddot{y}_2+\varepsilon_2\ddot{\theta}_2\cos\theta_2-\varepsilon_2\dot{\theta}_2^2\sin\theta_2)+c_2\dot{y}_2+c_m\dot{\delta}\cos\alpha+k_2y_2+k_m\delta\cos\alpha=0 \tag{35}$$

$$(I_2+m_2\varepsilon_2^2)\ddot{\theta}_2-m_2\varepsilon_2(\ddot{x}_2\sin\theta_2-\ddot{y}_2\cos\theta_2)+c_{t2}\dot{\theta}_2+c_mR_2\dot{\delta}+k_mR_2\delta=0 \tag{36}$$

4. Analysis of the dynamic responses

In order to verify the equations of motion derived in this paper, the time responses obtained from the proposed equations are compared to the time response from the equations of Umezawa et al. [17]. All the time responses in this study are computed by the Newmark method. Using the notations of this paper, the equations of motion presented by Umezawa et al. can be represented by

$$I_1\ddot{\theta}_1+c_{t1}\dot{\theta}_1+c_mR_1(R_1\dot{\theta}_1+R_2\dot{\theta}_2)+k_mR_1(R_1\theta_1+R_2\theta_2)=T \tag{37}$$

$$I_2\ddot{\theta}_2+c_{t2}\dot{\theta}_2+c_mR_2(R_1\dot{\theta}_1+R_2\dot{\theta}_2)+k_mR_2(R_1\theta_1+R_2\theta_2)=0 \tag{38}$$

The spur gear pairs have the rotating speed of 1700 rev/min, the gear mesh damping coefficient of c_m=10 N m/s, and the bearing damping coefficients $c_{t1}=c_{t2}$=10 N m s. The other material properties and dimensions have the same values as those of Ref. [17]. The main difference between the present study and Ref. [17] is whether the translational motions or shaft vibrations are considered or not. As seen in Eqs. (37) and (38), Umezawa et al. derived only the equations for rotational motion for spur gear pairs. The time responses for the acceleration of a point 7 cm apart from the pinion center are computed by using the equations of both Ref. [17] and the present study. The results of computations are plotted in Fig. 5, which shows some differences in the magnitudes of vibration. Comparing the results of Ref. [17] (Fig. 5(a)) with the results of the present study (Figs. 5(b) and (c)), the vibration amplitudes of the present study are relatively larger than those of Ref. [17]. The reason is because the present study includes the shaft vibration which is not considered in Ref. [17]. It is also observed from Figs. 5(b) and (c) that the vibration magnitude increases as the bearing stiffness decreases from $k_b=10^7$ to 10^6 N/m. Therefore, the spur gear set model of this study is more realistic than the model of Ref. [17].

For the dynamic analysis of spur gear pairs, more numerical computations are carried out and the dynamic responses of spur gears are obtained. The spur gear system used in computation has the following data. The tooth numbers for the pinion and the gear are 20 and 30, respectively. The initial pressure angle is given as 20°, while the initial distance between the centers of the pinion and the gear is given as 50 mm. On the other hand, the base pitch is 5.9 mm, and the torque applied to the pinion is 45 N m. The other parameters for the gear set are summarized in Table 1. In order to compute the time responses of the gear set, the time step size is selected as $\Delta t=10^{-9}$ s.

The dynamic responses of the proposed new model are compared to those of the previous model. As mentioned previously, the main difference is that the new model considers translational motion due to bearing deformation while the previous model does not. Therefore, the new model has a time-dependent pressure angle and contact ratio, while the previous model has a constant pressure angle and contact ratio. The difference between the new and previous models is shown in Fig. 6 which illustrates the time responses for mesh deformation. If the time axis of Fig. 6 is magnified, as shown in Fig. 7, some differences are observed in the mesh periods. In Fig. 7, T_1 and T_2 correspond to $(m_p-1)T_m$ and $(2-m_p)T_m$ of Fig. 4, respectively. T_1 and T_2 of the new model are different from those of the previous model, and the sum of T_1 and T_2 of the new model is also different from that of the previous model. This means that the new and previous models have different contact ratios and mesh periods during the gear set rotation.

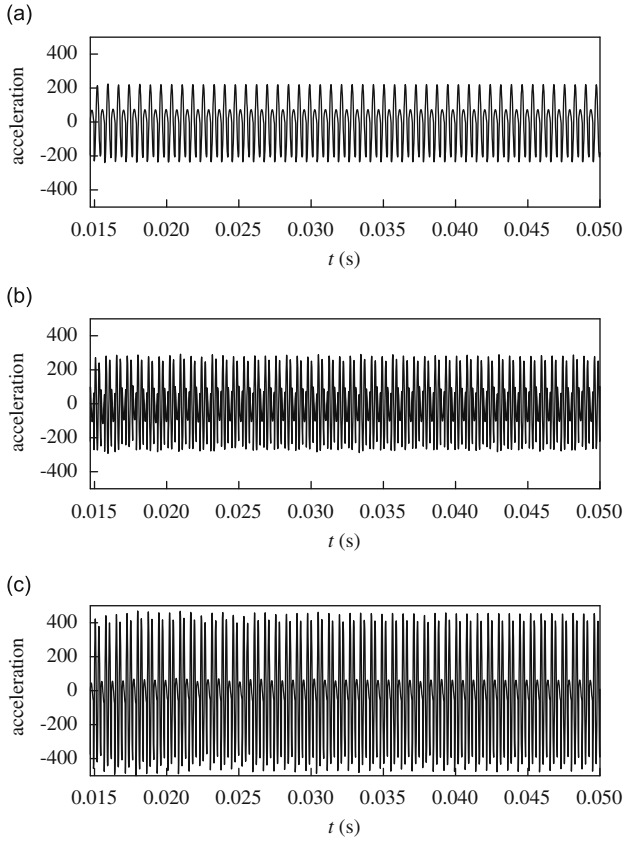

Fig. 5. Accelerations of a point 7 cm apart from the pinion center: (a) Umezawa et al. [17], (b) the present study when $k_b=10^7$ N/m, and (c) the present study when $k_b=10^6$ N/m.

Table 1
Gear set parameters.

	Pinion	Gear
Tooth number	20	30
Base circle radius (mm)	18.8	28.2
Addendum circle radius (mm)	22	32
Mass (g)	78.4	176.5
Mass moment of inertia (kg m^2)	1.39×10^{-5}	7.01×10^{-5}
Radial damping coefficient (N s/m)	5.6	8.4
Gear mesh damping coefficient (N s/m)	1.8	1.8
Torsional damping coefficient (N m s)	0.1	0.1
Bearing stiffness (N/m)	106	106
Mesh stiffness during one-pair contact (N/m)	0.75×10^8	0.75×10^8
Mesh stiffness during two-pair contact (N/m)	1.25×10^8	1.25×10^8

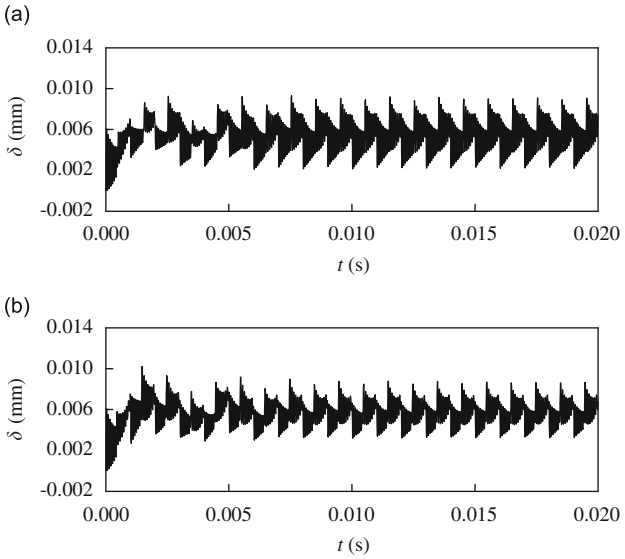

Fig. 6. Gear mesh deformations for the (a) new and (b) previous models.

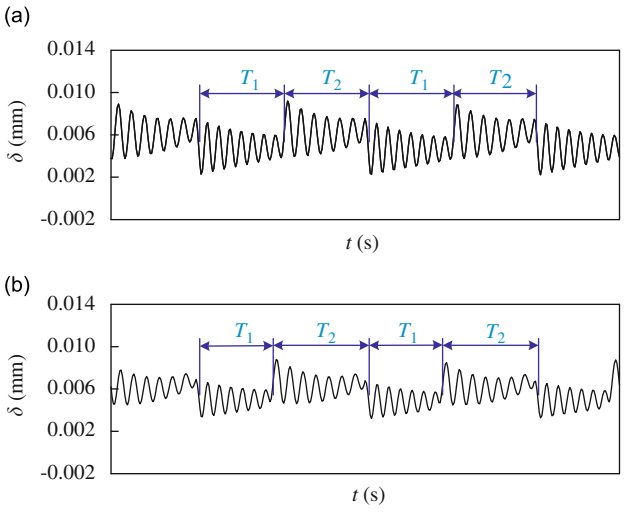

Fig. 7. Magnified gear mesh deformations for the (a) new and (b) previous models.

The differences can be also observed within the computed responses for the new and previous models, such as displacements and accelerations. Fig. 8 presents the differences in the radial displacements, r_1 and r_2, between the new and previous models. The radial displacements r_1 and r_2 are defined by $r_1=(x_1^2+y_1^2)^{1/2}$ and $r_2=(x_2^2+y_2^2)^{1/2}$, respectively. The respective differences between the new and previous models in r_1 and r_2 are denoted by Δr_1 and Δr_2. As seen in Fig. 8, the radial displacement of the pinion, r_1, has a larger difference between the new and previous models when compared to the displacement of the gear, r_2. The radial accelerations of the pinion for the new and previous models are plotted in Fig. 9, where a_{r1} and a_{r2} are the radial accelerations of the pinion and gear, respectively. The pinion acceleration obtained from the new model is very different from the acceleration obtained from the previous model. From the comparisons of the mesh deformations and the radial displacements/accelerations, it can be inferred that the new model is more accurate than the previous model because it considers the translational motion which is not considered in the previous model.

It is valuable to investigate the damping effects on the dynamic responses of the gear set. As mentioned before, the gear set has three kinds of damping: the radial bearing damping (c_1 and c_2), the gear mesh damping (c_m), and the torsional bearing damping (c_{t1} and c_{t2}). In order to analyze the damping effects, four cases of damping coefficients are discussed in this study. Case 1 considers all of the damping effects. The damping coefficients of this case are given by $c_1=5.6$, $c_2=8.4$, $c_m=1.8$ N s/m, and $c_{t1}=c_{t2}=0.1$ N m s. Case 2 has no radial bearing damping, so this case is defined by $c_1=c_2=0$, $c_m=1.8$ N s/m,

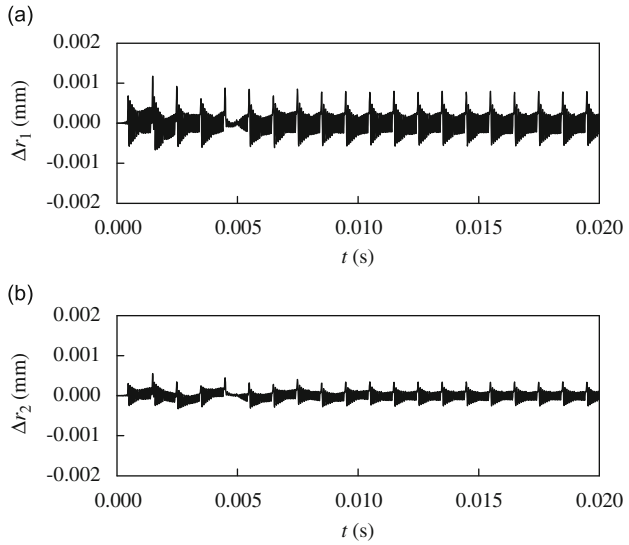

Fig. 8. Differences in the radial displacements between the new and previous models for (a) the pinion and (b) the gear.

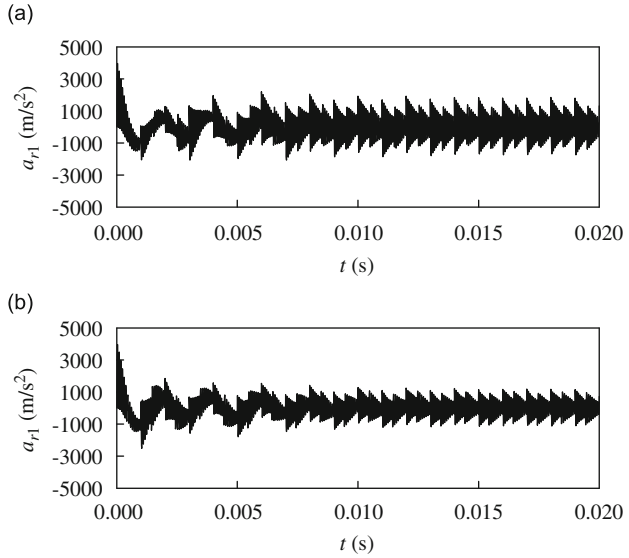

Fig. 9. Radial accelerations of the pinion in the (a) new and (b) previous models.

and $c_{t1}=c_{t2}=0.1$ N m s. Case 3 corresponds to the case without gear mesh damping having the values $c_1=5.6$, $c_2=8.4$, $c_m=0$ N s/m, and $c_{t1}=c_{t2}=0.1$ N m s. Case 4 involved no torsional bearing damping and is described by $c_1=5.6$, $c_2=8.4$, $c_m=1.8$ N s/m, and $c_{t1}=c_{t2}=0$. For these four cases, the dynamic responses for the radial displacements of the pinion are computed and plotted in Fig. 10. No difference in the radial displacements for Cases 1 and 3 is found. This implies that the gear mesh damping has little effect on the radial displacement. When comparing Cases 2 and 4, the torsional bearing damping has a larger influence on the radial displacement decrease, in comparison to that of the radial bearing damping. Consider the pinion subjected to constant torque M when the gear set has no torsional damping. In this case, the angular velocity of the pinion θ_1 monotonically increases with time. The reason is because the equation of motion for the pinion, Eq. (33), which has no term of θ_1, is a first-order differential equation with respect to$\dot{\theta}_1$. The radial displacement of the pinion, r_1, also increases with the angular velocity. Therefore, the torsional bearing damping has a great effect on the dynamics of the gear set.

The effects of bearing stiffness on radial displacement and gear mesh deformation are analyzed. Fig. 11 presents the time histories for the radial displacements of the pinion for the various values of bearing stiffness. As this figure shows, the vibration amplitude of the radial displacement increases as the bearing stiffness decreases. Another observation of Fig. 11 is that the period of radial vibration decreases with bearing stiffness. These behaviors of the radial displacement are expected. The gear mesh deformations caused by the variations in bearing stiffness are shown in Fig. 12. Figs. 12(a)–(c) correspond to the bearing stiffnesses of 10^6, 5×10^6, and 10^7 N/m, respectively. These figures demonstrate that an increase in bearing stiffness results in a small mesh deformation change. Therefore, it can be concluded from Figs. 11 and 12 that the bearing stiffness has a large effect on radial displacement, but it has only a small effect on mesh deformation.

The bearing stiffness also has an influence on the pressure angle and the contact ratio of spur gear pairs. For the bearing stiffness values of $k_b=10^6$, 5×10^6, and 10^7 N/m, the time histories for the pressure angle and contact ratio are plotted in Fig. 13. As shown in this figure, the fluctuation magnitudes of the pressure angle and contact ratio decrease with the bearing stiffness. This is easily expected because the shaft flexibility results in the changes of the pressure angle and contact ratio. However, it is interesting that the pressure angle decreases with the bearing stiffness while the contact ratio increases with the stiffness. Furthermore, the proposed model of this study enables to predict the amounts of pressure angle and contact ratio in a steady state. For example, the steady-state values of the pressure angle and contact ratio are given by 18.38° and 1.67, respectively, when $k_b=10^6$ N/m.

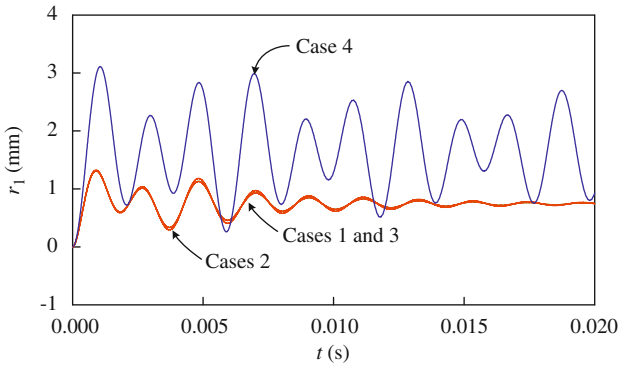

Fig. 10. Radial displacements of the pinion for the various values of damping coefficients: Case 1 ($c_1=5.6$, $c_2=8.4$, $c_m=1.8$ N s/m and $c_{t1}=c_{t2}=0.1$ N m s); Case 2 ($c_1=c_2=0$, $c_m=1.8$ N s/m and $c_{t1}=c_{t2}=0.1$ N m s); Case 3 ($c_1=5.6$, $c_2=8.4$, $c_m=0$ N s/m and $c_{t1}=c_{t2}=0.1$ N m s); and Case 4 ($c_1=5.6$, $c_2=8.4$, $c_m=1.8$ N s/m, $c_{t1}=c_{t2}=0$).

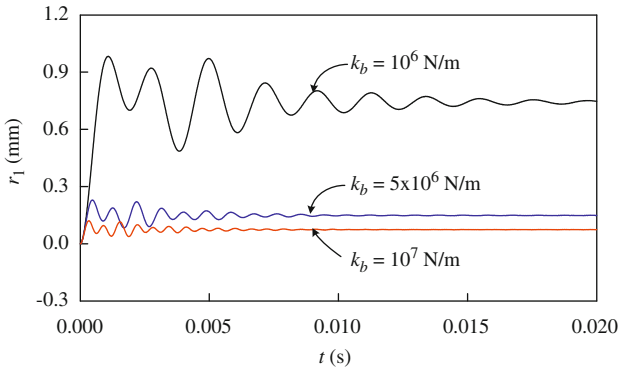

Fig. 11. Radial displacements of the pinion for the various values of bearing stiffness.

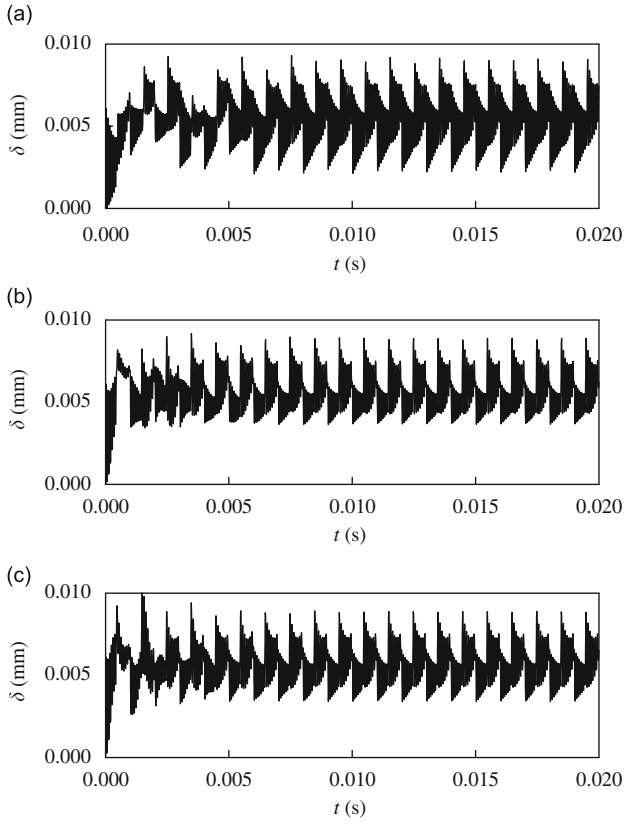

Fig. 12. Gear mesh deformations for the various values of bearing stiffness: (a) k_b=10^6, (b) k_b=5 × 10^6, and (c) k_b=10^7 N/m.

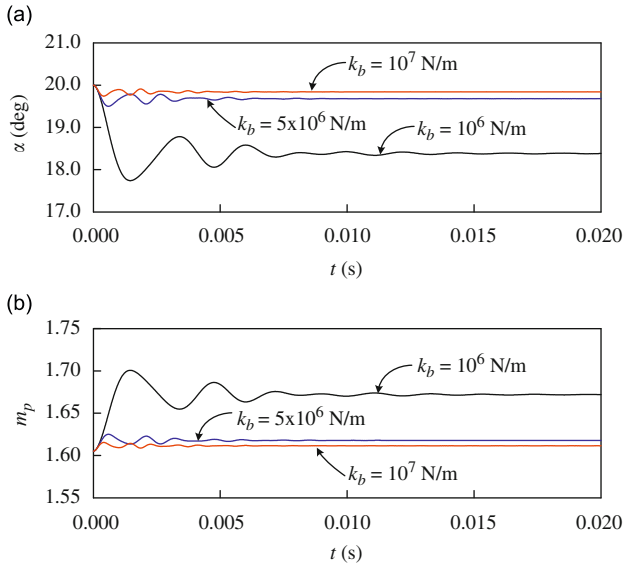

Fig. 13. Pressure angle and contact ratio for the various values of bearing stiffness: (a) pressure angle and (b) contact ratio.

In order to examine the influence of gear mesh stiffness on radial displacement and gear mesh deformation, the radial displacements and the mesh deformations are computed for three cases of mesh stiffness. Case 1 is for k_l=0.55 × 10^8 and k_u=0.77 × 10^8 N/m, Case 2 is for k_l=1.07 × 10^8 and k_u=1.53 × 10^8 N/m, and Case 3 is for k_l=5.05 × 10^8 and k_u=7.31 × 10^8 N/m. Cases 1, 2, and 3 correspond to Young's modulus of the gear system material 45 × 10^9, 21 × 10^{10}, and 105 × 10^{10} Pa, respectively. As shown in Fig. 14, Cases 2 and 3 have no noticeable difference in radial displacement; however, Case 1 has a

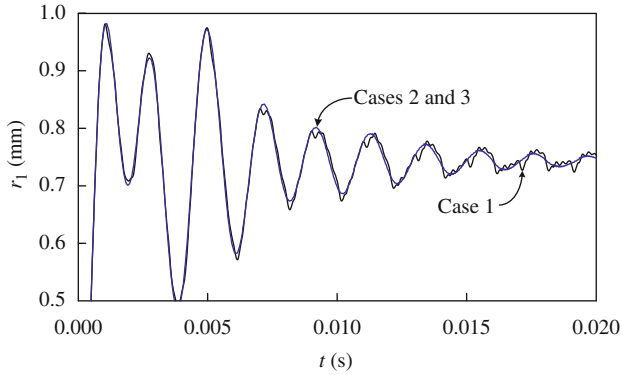

Fig. 14. Radial displacements of the pinion for the various values of mesh stiffness: Case 1 (k_l=0.55 × 10^8, k_u=0.77 × 10^8 N/m); Case 2 (k_l=1.07 × 10^8, k_u=1.53 × 10^8 N/m); and Case 3 (k_l=5.05 × 10^8, k_u=7.31 × 10^8 N/m).

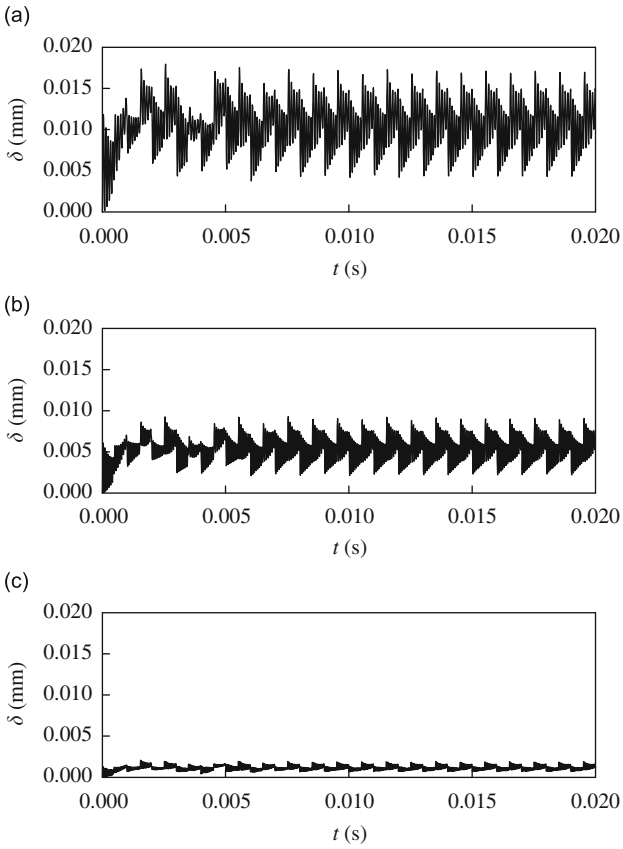

Fig. 15. Gear mesh deformations of the pinion for the various values of mesh stiffness: Case 1 (k_l=0.55 × 10^8, k_u=0.77 × 10^8 N/m); Case 2 (k_l=1.07 × 10^8, k_u=1.53 × 10^8 N/m); and Case 3 (k_l=5.05 × 10^8, k_u=7.31 × 10^8 N/m).

relatively high-frequency vibration in comparison to those of Cases 2 and 3. In Fig. 15, the gear mesh deformations are plotted for the above three cases. The mesh deformation of Case 1 is much larger than those of Cases 2 and 3. Therefore, it can be induced that the high-frequency vibration of Case 1 shown in Fig. 14 originates from gear mesh deformation.

5. Summary and conclusions

In this study, the dynamic behaviors of a pair of spur gears were analyzed with translational motion due to bearing deformation. When considering translational motion, a new model for a pair of spur gears was proposed, and then the nonlinear equations of motion were derived. Based on the equations of motion, the dynamic responses were computed by

applying the Newmark time integration method. Furthermore, this paper presents the influences of various mechanical properties such as damping and stiffness on the dynamic responses.

The results of this study can be summarized as follows:

(1) The proposed new model has a time-dependent pressure angle and contact ratio; therefore, the new model produces a more accurate dynamic response than does the previous model.
(2) The gear mesh damping has little effect on the dynamic responses for the radial displacements of a gear set.
(3) The torsional bearing damping has a stronger effect on the dynamic responses of a gear set than does the radial bearing damping.
(4) The bearing stiffness has a significant effect upon both the amplitude and period of the radial vibration of a gear set, but has little effect on the mesh deformation.
(5) The increase in gear mesh stiffness causes decreases in the amplitude and period of the vibration of the gear mesh deformation; however, the mesh stiffness has little effect on the radial vibration of a gear set.
(6) The pressure angle decreases and the contact ratio increases as the bearing stiffness increases.

References

[1] R.W. Cornell, Compliance and stress sensitivity of spur gear teeth, *Journal of Mechanical Design, Transaction of ASME* 103 (2) (1981) 447–459.
[2] M.S. Tavakoli, D.R. Houser, Optimum profile modifications for the minimization of static transmission errors of spur gears, *Journal of Mechanisms Transmissions and Automation in Design, Transaction of ASME* 108 (1) (1986) 86–95.
[3] K.J. Huang, T.S. Liu, Dynamic analysis of a spur gear by the dynamic stiffness method, *Journal of Sound and Vibration* 234 (2) (2000) 311–329.
[4] J.H. Kuang, A.D. Lin, Theoretical aspects of torque responses in spur gearing due to mesh stiffness variation, *Mechanical Systems and Signal Processing* 17 (2) (2003) 255–271.
[5] M. Amabili, A. Fregolent, A method to identify modal parameters and gear errors by vibrations of a spur gear pair, *Journal of Sound and Vibration* 214 (2) (1998) 339–357.
[6] A. Kahraman, Load sharing characteristics of planetary transmissions, *Mechanism and Machine Theory* 29 (8) (1994) 1151–1165.
[7] A. Kahraman, G.W. Blankenship, Effect of involute contact ratio on spur gear dynamics, *Journal of Mechanical Design, Transaction of ASME* 121 (1) (1999) 112–118.
[8] P. Velex, M. Maatar, A mathematical model for analyzing the influence of shape deviations and mounting errors on gear dynamic behavior, *Journal of Sound and Vibration* 191 (5) (1996) 629–660.
[9] P. Velex, M. Ajmi, Dynamic tooth loads and quasi-static transmission errors in helical gears—approximate dynamic factor formulae, *Mechanism and Machine Theory* 42 (11) (2007) 1512–1526.
[10] H.N. Ozguven, D.R. Houser, Dynamic analysis of high speed gears by using loaded static transmission error, *Journal of Sound and Vibration* 125 (1) (1998) 71–83.
[11] A. Kahraman, R. Singh, Nonlinear dynamics of a spur gear pair, *Journal of Sound and Vibration* 142 (1) (1990) 49–75.
[12] A. Kahraman, R. Singh, Nonlinear dynamics of a geared rotor-bearing system with multiple clearances, *Journal of Sound and Vibration* 144 (3) (1991) 469–506.
[13] J. Lin, R.G. Parker, Mesh stiffness variation instabilities in two-stage gear systems, *Journal of Vibration and Acoustics, Transaction of the ASME* 124 (1) (2002) 68–76.
[14] A. Kahraman, Effect of axial vibrations on the dynamics of a helical gear pair, *Journal of Vibration and Acoustics, Transaction of ASME* 115 (1) (1993) 33–39.
[15] N.M. Newmark, A method of computation for structural dynamics, *Journal of the Engineering Mechanics Division, Proceedings of ASCE* 85 (EM3) (1959) 67–94.
[16] F. Chaari, W. Baccar, M.S. Abbes, M. Haddar, Effect of spalling or tooth breakage on gearmesh stiffness and dynamic response of a one-stage spur gear transmission, *European Journal of Mechanics–A/Solid* 27 (2008) 691–705.
[17] K. Umezawa, T. Sato, J. Ishikawa, Simulation of rotational vibration of spur gears, *Bulletin of JSME* 27 (1984) 102–109.